


Article

Formation Mechanism and Modeling Method of Wrinkling Defects in Variable Angle Tow Steering Fiber Placement

Minghui Yi ¹, Fei Liu ¹, Wuxiang Zhang ^{1,2,*}  and Xilun Ding ^{1,2}
¹ School of Mechanical Engineering and Automation, Beihang University, 37 Xueyuan Road, Beijing 100191, China

² Ningbo Institute of Technology, Beihang University, Ningbo 315832, China

* Correspondence: zhangwuxiang@buaa.edu.cn

Abstract: Variable angle tow steering technology is capable of manufacturing complex aviation parts with a trajectory of intricate curvature planned based on stress or profile characteristics, which greatly improves the forming efficiency, design flexibility and mechanical properties of composite structures. In view of the forming defects such as buckling and wrinkles caused by the lateral bending of fiber prepreg tow, a theoretical buckling model based on the Rayleigh Ritz method, the principle of minimum potential energy and the viscoelastic foundation is established, in which the adhesion coefficient is characterized by the degree of intimate contact to introduce process parameters. On the basis of the contact mechanics analysis, the distribution of the compaction pressure and bending stress is studied to improve the theoretical model, and the critical buckling load and the minimum radius of the tow under the normal and tangential contact conditions are determined precisely. Finally, the finite element models of compaction and variable angle steering placement are proposed, and the theoretical model and simulation model are verified by corresponding trials. It is demonstrated that defects can be effectively suppressed through optimizing process parameters.

Keywords: variable angle tow steering; buckling model; contact mechanics; defects suppression



Citation: Yi, M.; Liu, F.; Zhang, W.; Ding, X. Formation Mechanism and Modeling Method of Wrinkling Defects in Variable Angle Tow Steering Fiber Placement. *Aerospace* **2022**, *9*, 620. <https://doi.org/10.3390/aerospace9100620>

Academic Editor: Konstantinos Kontis

Received: 31 August 2022

Accepted: 14 October 2022

Published: 19 October 2022

Publisher's Note: MDPI stays neutral with regard to jurisdictional claims in published maps and institutional affiliations.



Copyright: © 2022 by the authors. Licensee MDPI, Basel, Switzerland. This article is an open access article distributed under the terms and conditions of the Creative Commons Attribution (CC BY) license (<https://creativecommons.org/licenses/by/4.0/>).

1. Introduction

Advanced composite materials with carbon fiber as a reinforcement have had high performance advantages in specific strengths and specific stiffnesses since their first application in the field of aircraft manufacturing in the early 1970s. It can reduce the weight of aircraft by 10–40% and the cost of structural design by 15–30%, which plays a vital role in the lightweight and modularization of the aircraft structure [1]. As one of the most advanced composite structure-forming technologies at present, automated fiber placement (AFP) can realize the multi-fiber prepreg tows to be laid on the mold surface layer by layer according to the preset trajectory, while taking into account the production efficiency and the complexity of products. Compared with manual laying, filament winding, automated tape laying and other methods, AFP has lower cost and higher flexibility [2,3], which has been widely used in the forming and manufacturing of aerospace composite structures.

Variable angle composite (VAC) [4], first proposed in 1992, can improve the mechanical properties of the structure and relieve the local stress concentration without increasing the weight [5], promoting the design and application of composite laminated structures with variable thicknesses and stiffnesses in aerospace and other fields [6–8]. Variable angle tow steering (VATS) combines AFP with the VAC structure, which is suitable for high-performance manufacturing of complex aircraft structures, such as hyperbolic blended wing bodies, s-shaped air inlets and engine fan blades. However, the compression performance of carbon fiber composites is worse than the tensile performance, and buckling occurs on the compressed side in virtue of the accumulated strain energy overcoming the adhesion [9,10], resulting in equally spaced wrinkles [11]. Devesh systematically presented the multiple

types of defects [12] associated with the manufacturing processes in curvilinear fiber placement, including but not limited to wrinkles, waviness, overlaps, etc.

In order to explore the formation mechanism and suppression method of buckling defects in VATS, Beakou [13] established a mathematical model based on elastic orthotropic rectangular thin plates and used independent elastic elements to represent the bonding performance of prepreg tow. To narrow the gap between the above model and actual working conditions, Matveev added a simple boundary condition [14] to the model and modified the deflection equation to make the solved critical load formula more convincing. The models they established are relatively simple, and the deflection equation cannot meet the boundary conditions in VATS. Belhaj perfected the composition of the model by introducing the shear ply [15] between the prepreg tow and elastic elements to simulate the interaction between the elements, and derived the differential control equation of axisymmetric buckling of the thin plate with variable stiffness without verification, which led to the complexity of the model. Nima [16] proposed a modeling method to characterize the blisters and wrinkles during tow steering and obtained the simulation results, but lacked corresponding theoretical model support. For the wrinkling in bilayer systems, Huang et al. established a model for evolving wrinkles consisting of an elastic layer and a viscoelastic layer [17–19].

However, most of the current buckling models are based on the minimum potential energy principle of thin plates, in which the boundary conditions and deflection functions are not accurate and there is a lack of correspondence with the placement process conditions. Moreover, the compaction and rotating traction effects of the compaction roller on the prepreg tow in VATS are ignored, which affect the stress-strain state and the adhesion performance of the layer, thus affecting the magnitude and distribution accuracy of the deflection. In addition, there is a lack of accurate simulation analysis methods for VATS, which is not conducive to the efficient verification and iterative optimization of the buckling theoretical model.

In this paper, a theoretical model of buckling defects in VATS based on the theory of plates and shells is proposed. The viscoelastic elements are used to characterize the bonding performance between the tow and the mold, and the boundary conditions of large deflection bending of the elastic thin plate are determined according to their actual condition. The detailed modeling process is introduced in Section 2. Secondly, based on Hertz's contact principle, the normal contact and tangential contact models of the flexible compaction roller and prepreg tow are established, and the distribution of compaction pressure on the surface of the tow and the internal stress in the section of the tow are solved in Section 3, resulting in the critical buckling load and the minimum lateral bending radius. In Section 4, finite element software is used to establish the simulation model of VATS to verify the distribution of compaction pressure, in-plane compression load and the formation of defects such as wrinkles. In Section 5, the theoretical model and simulation model are verified by experiments, and the influence mechanism of process parameters on defects in VATS is explored, so as to prove the feasibility of optimizing process parameters to suppress the forming defects. Finally, Section 6 summarizes the research contents of this paper and makes some concluding remarks.

2. Modeling of Defects Formation in VATS

The main reason for the out of plane wrinkles in VATS is the mismatch between the length of trajectory and the initial length of the tow, resulting in the tensile and compressive combined load along the width direction in the section of prepreg. In this paper, the formation mechanism of wrinkle defects under non-uniform load is studied, which is approximated as a large deflection buckling model of a thin plate laid on a viscoelastic foundation and is solved by accurate boundary conditions and the deflection function.

2.1. Viscoelastic Foundation and Boundary Conditions

It is known that the deflection is much larger than the thickness of the tow, and the curvature of the trajectory is relatively small. Therefore, the buckling tow is equivalent to a rectangular orthotropic homogeneous flexible thin plate, and the buckling equation is established by the large deflection bending theory of the thin plate. The uniformly distributed elastic elements are used to characterize the inhibition effect of the adhesion between the tow and the mold on the formation of wrinkles (Figure 1); that is, the adhesive layer composed of spring elements is inserted, and its elastic coefficient represents the adhesion force of the tow, which is directly affected by process parameters.

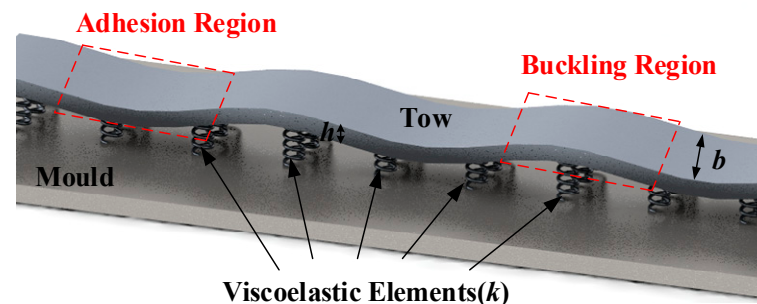


Figure 1. Diagram of the buckling model based on elastic foundation.

First of all, the large deflection bending theory of elastic thin plates is based on the Kirchhoff hypothesis; that is, there is a neutral plane without in-plane deformation, and the rest of the plate is parallel to the plane of the neutral plane, which remains parallel after bending. The compaction roller applies torque to the tow, and both sides of the neutral plane are in tension and compression, respectively, while the neutral plane stress is 0. It is assumed that the edge of the tow under the roller is fixed without deformation to ensure that the load in the section is linearly distributed along the width direction.

Before establishing the buckling model, it is necessary to determine the boundary conditions of the elastic thin plate. The two edges (Edge 1 and Edge 2) along the fiber length direction are fixed support edges, and there are no wrinkles at the boundary positions. Among them, the strain energy stored at Edge 1 is not enough to overcome the adhesion force to delaminate the tow. Edge 2 is the real-time compaction position, which bears the normal compaction load and in-plane torque. Therefore, the two boundaries and the nearby small area are in good contact with the mold. Because the axial tensile strength of the prepreg fiber tow is large, the outer boundary keeps in contact with the mold, and the wrinkles appear at the inner boundary. Macroscopically, it appears as a small rotation around the outer boundary and away from the mold. Consequently, the outer boundary (Edge 3) is simply supported, and the inner boundary (Edge 4) is a free edge with approximately equidistant wrinkles after compression buckling.

The kinematic boundary conditions of the thin plate model are:

$$\begin{aligned} \omega(x=0) &= 0 \quad \omega'(x=0) = 0 \\ \omega(x=L) &= 0 \quad \omega'(x=L) = 0 \\ \omega(y=b) &= 0 \quad \omega''(y=b) = 0 \end{aligned} \quad (1)$$

where ω is the buckling deflection, L is the length of the buckling model and b is the width.

The load boundary conditions of the buckling model are complex. Edge 1 is a fixed boundary, and its stress has no effect on the establishment of the model. Edge 2 bears the coupling load of compression and torsion from the roller, wherein the compaction force has a direct impact on the adhesion coefficient of the tow, and the torque is applied in the cross-section of the tow and is approximately expressed as the in-plane tensile and compressive load perpendicular to the boundary. Edge 3 only bears the support force from the mold, while Edge 4 is a free boundary without any load.

2.2. Optimized Buckling Model Based on Rayleigh Ritz Method

The flow of the Ritz method to solve the large deflection buckling equation of the thin plate is as follows: firstly, the buckling deflection function ω is assumed to satisfy all boundary conditions; the total potential energy of the large deflection buckling model is solved, including the elastic strain energy, the potential energy of the viscoelastic elements and the work done by the in-plane load; according to the principle of minimum potential energy (the first-order variation of the total potential energy is 0), the critical load, i.e., the maximum compression load in the plane of the inner boundary, is solved; finally, the critical torque and the minimum radius of curvature are obtained based on the critical load.

Since the established buckling model is a rectangular thin plate structure with fixed support on opposite sides and a simple support on one side, the Navier method [13] and Levy method [14] based on Fourier trigonometric function series cannot meet the boundary conditions. In this paper, a deflection function based on the deformation form of the double cosine series is proposed:

$$\omega(x, y) = \sum_{m=1}^{\infty} \sum_{n=1}^{\infty} a_{mn} \left(1 - \cos \frac{2m\pi x}{L}\right) \cos \frac{(2n-1)\pi y}{2b} \quad (2)$$

where a_{mn} is the Fourier coefficient.

The deflection function Equation (2) has different frequencies along the X direction (fiber length) and the Y direction (fiber width), which ensures that the deflection, rotation angle and bending moment of the thin plate at the boundary meet the requirements.

The strain potential energy of the thin plate model is:

$$U(\omega) = \frac{1}{2} \int_0^L \int_0^b \left[D_{11} \left(\frac{\partial^2 \omega}{\partial x^2} \right)^2 + D_{22} \left(\frac{\partial^2 \omega}{\partial y^2} \right)^2 + 2D_{12} \frac{\partial^2 \omega}{\partial x^2} \frac{\partial^2 \omega}{\partial y^2} + 4D_{66} \left(\frac{\partial^2 \omega}{\partial x \partial y} \right)^2 \right] dx dy \quad (3)$$

where D_{ij} is the bending stiffness of the tow.

The potential energy of the elastic elements is:

$$V(\omega) = \frac{1}{2} \int_0^L \int_0^b k \cdot \omega^2 dx dy \quad (4)$$

where k is the adhesion coefficient of the prepreg tow.

The work done by the in-plane load is:

$$W(\omega) = \frac{1}{2} \int_0^L \int_0^b N_x \left(\frac{\partial \omega}{\partial x} \right)^2 dx dy \quad (5)$$

where N_x is the in-plane load of Edge 2.

$$N_x(y) = \frac{2N_0}{b} y - N_0 \quad (6)$$

where N_0 is the boundary load.

Assuming that the tensile and compressive loads are equal and the directions are opposite, the in-plane load is linearly distributed along the tow width direction (Figure 2).

According to the Rayleigh–Ritz method, the total potential energy of the buckling model system is:

$$\Pi(\omega) = U(\omega) + V(\omega) - W(\omega) \quad (7)$$

Substitution of Equations (2)–(6) into Equation (7), the total energy of the theoretical model is:

$$\Pi = \frac{Lb}{8} \left[D_{11} a_{mn}^2 \left(\frac{m\pi}{L} \right)^4 + D_{22} a_{mn}^2 \left(\frac{n\pi}{b} \right)^4 + 2D_{12} a_{mn}^2 \left(\frac{mn\pi^2}{Lb} \right)^2 + 4D_{66} a_{mn}^2 \left(\frac{mn\pi^2}{Lb} \right)^2 + k a_{mn}^2 - a_{mn}^2 \left(\frac{m\pi}{L} \right)^2 \frac{N_0}{n^2 \pi^2} \right] \quad (8)$$

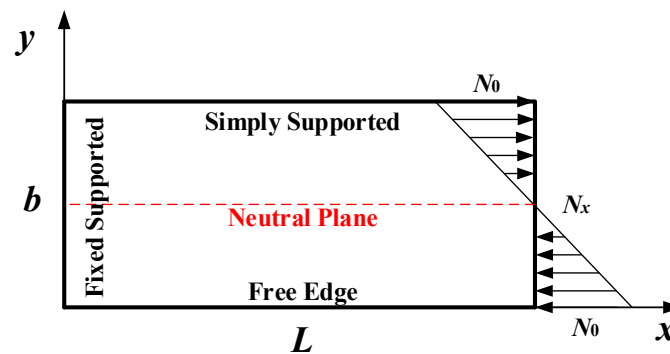


Figure 2. Distribution of applied in-plane stress.

According to the principle of minimum potential energy, the first-order variation of the total energy equation is 0, and only the first-order deflection equation is selected for calculation in this paper. The prepreg fiber tow is highly anisotropic, and the bending stiffness in other directions is much smaller than D_{11} . The critical buckling load of the prepreg tow can be obtained:

$$N_{0cr} = D_{11} \frac{\pi^4}{L^2} + kL^2 = \frac{\pi^4 E_1 b h^3}{12 L^2} + kL^2 \quad (9)$$

where h is the thickness of the prepreg tow and E_1 is the Young's modulus.

It can be seen from Equation (8) that there are many factors affecting the buckling state of the inner side. In addition to the material properties (width, thickness and Young's modulus of the tow), the in-plane compression load and the adhesion coefficient between the tow and the mold play an important role. Therefore, in this paper, intimate contact is used to characterize the adhesion coefficient, and the rough surface of the prepreg tow is equivalent to a rectangular element array with equal spacing distribution (Figure 3). The fluid continuity equation is used to calculate the geometric size change of rectangular elements before and after compaction, which is the evaluation index for the bonding effect of the layers [20–22].

The expression of intimate contact degree is as follows:

$$D_{ic} = \frac{1}{1 + \frac{w_0}{b_0}} \left[1 + 5 \left(1 + \frac{w_0}{b_0} \right) \left(\frac{a_0}{b_0} \right)^2 \frac{P}{\mu_{mf}} t_{ic} \right]^{1/5} = \alpha \left(\frac{P}{\mu_{mf}} t_{ic} \right)^{1/5} \quad (10)$$

where a_0 , b_0 and w_0 are the characteristic parameters of the surface roughness of the prepreg tow, which can be simplified as α , P is the compaction pressure on the tow surface, t_{ic} is the contact time between the tow and the roller, and μ_{mf} is the resin viscosity related to temperature.

The compaction pressure and in-plane compression load of the prepreg tow have a strong correlation with the formation of buckling defects, and the above loads are all from the contact between the compaction roller and the tow. Wherein the compaction pressure is derived from the normal force applied by the roller to the tow through the normal contact, and the in-plane load comes from the tangential contact force exerted by the roller on the tow. The contact model between the compaction roller and the tow will be described in detail in Section 3.

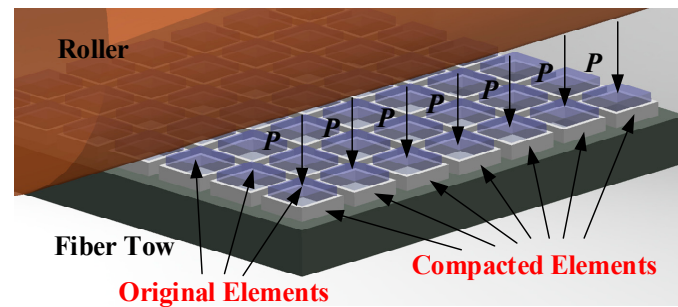


Figure 3. Diagram of intimate contact.

3. Modeling of the Contact between Compaction Roller and Tow

In the VATS process, the robot applies a preset compaction force to the prepreg tow through the compaction roller, and the flexible roller will deform to a certain extent under the pressure, forming a compaction region of a certain width so that the layers have a better bonding effect. Simultaneously, the robot end effector drives the placement head to rotate around the normal line of the laying surface while maintaining the compaction state. The friction force between the roller and the tow in the compaction region drives the tow to bend laterally, so that the tow can be laid continuously in a curve with variable angles.

3.1. Normal Contact Model Based on Hertz Theory

The contact model between the flexible roller and the prepreg tow can be divided into the contact along the tow length direction and the contact along the tow width direction [23]. Since the roller continuously compacts the tow on the mold surface along the laying direction, the compaction effect on each position of the tow is consistent; that is, the tow is laid under the maximum pressure. If the width of the tow is narrow, there is almost no difference in the pressure along the width of the tow. Consequently, the lateral and longitudinal distribution of the pressure have no impact on laying quality. The compaction model established in this paper is mainly to solve the maximum compaction pressure and the width of the contact region, so as to obtain the degree of intimate contact.

According to the Hertz contact theory [24], the compaction process of the prepreg tow by a flexible roller can be simplified by the contact model of an elastic cylinder and a rigid half space (Figure 4). F is the compaction force applied by the robot, P is the pressure experienced by the prepreg tow, R is the radius of the compaction roller, h is the deformation depth of the flexible roller, d_1 is the width of the roller, and d_2 is the width of the contact region.

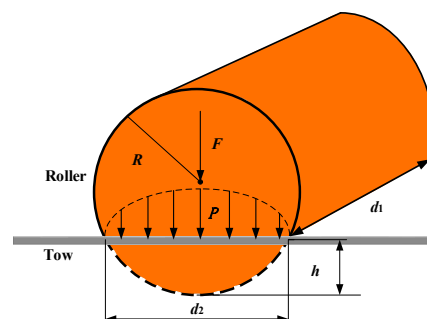


Figure 4. Schematic diagram of the Hertz contact.

The deformation depth is linearly proportional to the compaction force:

$$F = \frac{\pi}{4} E^* d_1 h \quad (11)$$

where $E^* = \frac{E_2}{1-\nu^2}$, E_2 is the elastic modulus of the roller material and ν is Poisson's ratio.

The width of the contact region is:

$$d_2 = 2\sqrt{Rh} = 4\sqrt{\frac{FR}{\pi E^* d_1}} \quad (12)$$

The compaction pressure is:

$$P = \sqrt{\frac{E^* F}{\pi d_1 R}} \quad (13)$$

Substituting Equations (11)–(13) into Equation (10), a new expression of the degree of intimate contact is obtained:

$$D_{ic} = \alpha \left(\frac{4F}{\mu_{mf} \pi d_1 V} \right)^{1/5} \quad (14)$$

The adhesion coefficient is expressed as:

$$k = \beta \left(\frac{4F}{\mu_{mf} \pi d_1 V} \right)^{1/5} \quad (15)$$

where β is constant and V is the laying speed.

The adhesive coefficient Equation (15) is brought into Equation (9) to obtain the expression of critical buckling load:

$$N_{0cr} = \frac{\pi^4 E_1 b h^3}{12 L^2} + \beta \left(\frac{4F}{\mu_{mf} \pi d_1 V} \right)^{1/5} L^2 \quad (16)$$

3.2. Tangential Contact Model Based on Torsion without Sliding

In the compaction region, the prepreg tow is subjected to a certain angle of lateral bending due to the tangential friction of the roller, which makes the tow lie in a continuous variable angle curve on the whole. The thickness of the tow is small, and it can be considered that the shear stress of the tow section is uniformly distributed along the thickness direction. Therefore, the tangential friction force of the tow surface forms the in-plane tensile and compressive loads (uniformly distributed along the thickness direction and linearly distributed along the width direction) in the tow section.

According to the friction contact theory, the tangential contact model between the roller and the tow is established (Figure 5), as well as the functional relationship between the total rotating torque of the placement head and the in-plane load. The width of the tow is small and close to the width of the compaction region. The tangential contact region can be approximated as a circular contact model, and the diameter is the width d_1 of the tow. In Figure 5, M is the torque applied to the roller, and N_0 is the in-plane compression and tensile load. In order to simplify the model, the relative sliding between the roller and the tow is not considered in this paper.

The simplified two-dimensional tangential contact model is a circular contact surface, and the polar radius of the contact region is $d_1/2$. The in-plane load is generated by the torsion of the roller compacted on the surface of the tow, which is perpendicular to the polar radius and linearly distributed along the radial direction. The total torque of the compaction roller acting on the contact region is:

$$M = \frac{1}{6} \pi d_1^3 N_0 \quad (17)$$

The buckling radius of the prepreg tow can be obtained by Equation (17) and the bending moment formula:

$$r_{cr} = \frac{E_1 b^3 h}{2 \pi d_1^3 N_{0cr}} \quad (18)$$

In the next section, the finite element software is used to establish a simulation model to verify the contact model and the distribution of the compaction force, analyze the tangential stress and the forming defects in VATS, and establish the corresponding relationship between the material parameters and the critical buckling radius based on the theoretical model.

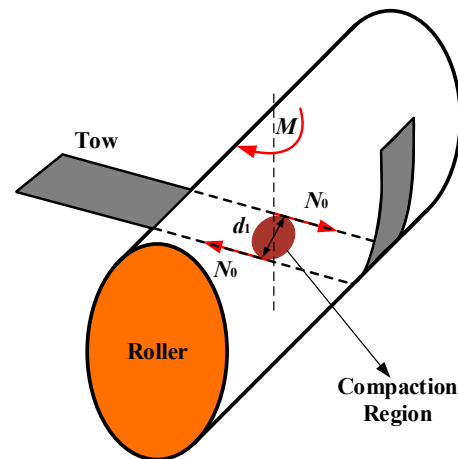


Figure 5. Schematic diagram of the tangential contact.

4. Simulation Modeling and Numerical Results Analysis

In this paper, the finite element software ANSYS [25] is used to establish the contact model between the roller and the prepreg tow. The VATS buckling simulation model established in this paper includes four parts: a deformable silicone rubber compaction roller (40 mm diameter, 30 mm width, 6.1396 MPa elastic modulus and 0.48 Poisson's ratio), an epoxy resin prepreg tow (6.35 mm width and 230 GPa elastic modulus), a rigid laying mold (structural steel) and a rigid roller mandrel (structural steel). In addition, the influence of important material parameters such as length, width and thickness of prepreg tow on critical buckling radius in the theoretical model is also studied in this section.

4.1. Simulation Model of Normal Contact and Pressure Distribution

The compaction force is generated by the robot end effector and applied to the mandrel of the roller, which then acts on the surface of the prepreg tow through the roller. Therefore, the compaction force applied to the rigid mandrel in the simulation model is closer to the actual situation. A small tensile force is applied to the upper section of the tow to simulate the tow tension and avoid the lateral slip of the tow. The established compaction simulation model is shown in Figure 6.

Since the model is mainly used to study the normal contact mechanism between the roller and the tow, the radial deformation of the roller and the distribution of the compaction force, the contact type between the roller and the tow, and the tow and the forming mold is set as fixed contact for the simplification of calculation; that is, the tangential relative displacement is not considered.

From the simulation results of normal contact (Figure 7), it can be seen that after the compaction force is applied, and the flexible roller deforms, forming a contact region approximately rectangular on the surface of the tow and the mold, and the maximum pressure is located at the center of the region. When the applied force is 50 N, the maximum compaction pressure at the center of the contact region is 0.46509 MPa, and the change is small within the tow width. The maximum theoretical compaction pressure calculated by Equation (13) is 0.46001 MPa, which is similar to the simulation result. The strain simulation results of the roller show that the width of the contact region is about 4.9081 mm after the roller is deformed, and the theoretical value of the width calculated by Equation (12) is 4.6130 mm.

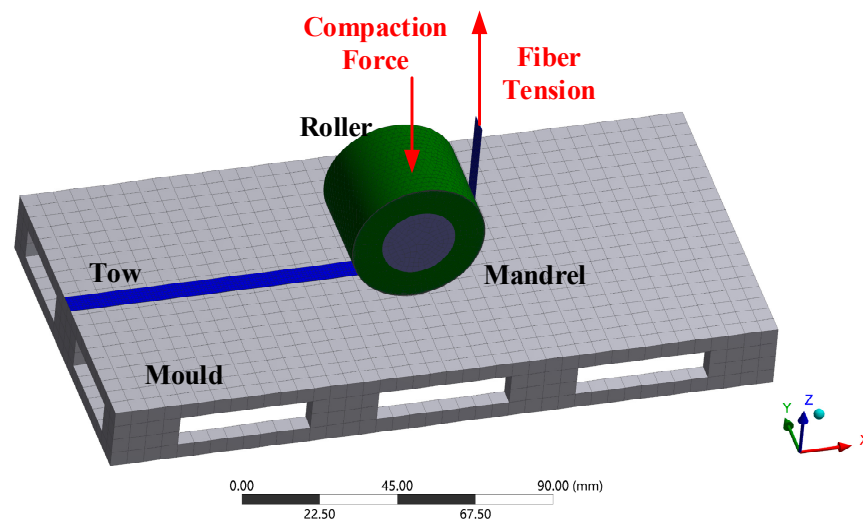


Figure 6. Simulation model of compaction contact.

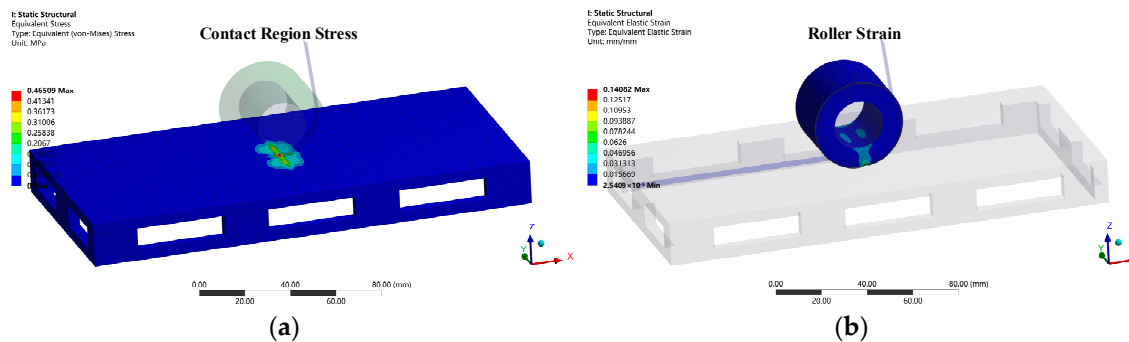


Figure 7. Nephogram of finite element simulation results: (a) Simulation results of contact stress; (b) Simulation results of roller strain.

By observing the stress and strain nephogram of the flexible compaction roller, it can be concluded that the normal contact stress and strain are distributed in a parabolic curve along the width direction, which is consistent with the theoretical equation of pressure distribution and further proves the feasibility of applying Hertz theory to the compaction contact model.

4.2. Simulation Model of Angular Contact and Buckling

The key to establishing the buckling simulation model in VATS is to determine the characterization method of the adhesion coefficient between the prepreg tow and the mold. Since the adhesion can inhibit the occurrence of buckling, delamination and other defects of the tow, it can be regarded as a connection mode between the tow and the mold. Therefore, this paper simulates the adhesion (tackiness of prepreg tow) with reference to the interface crack failure form of the adhesive structure. The interface delamination simulation methods in ANSYS software include virtual crack closure technology (VCCT) and cohesive zone materials (CZM).

Considering that the wrinkle area is unknown, it is impossible to set the preformed crack, so CZM is utilized to simulate the delamination. In order to simplify the simulation model, contact debonding is used to establish the contact pair between the tow and the mold, and different adhesion coefficients are characterized by setting the material properties of the cohesive zone (maximum normal contact stress and delamination gap) in the ACP pretreatment module. The Figure 8 shows the detailed modeling process.

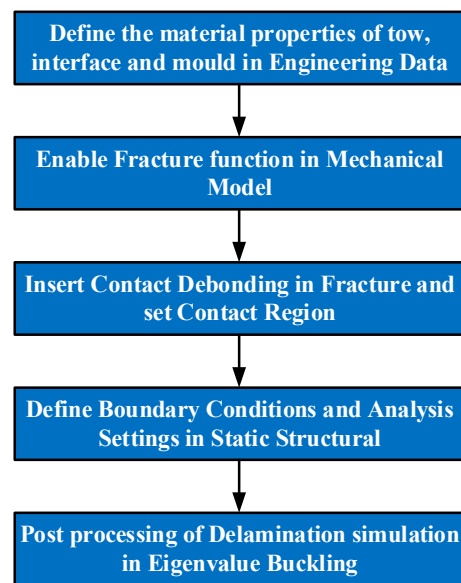


Figure 8. Flow chart of delamination simulation.

Firstly, the internal stress model of the tangential contact surface is verified. The laid edge of the prepreg tow is set as a fixed boundary, and a torque of 1 N·m is applied to the edge to be laid. Cohesive contact elements are established between the tow and the mold, and the equivalent stress simulation result (Figure 9) is 7.5702 MPa. The theoretical value of the maximum in-plane load (boundary load) calculated according to the functional relationship between torque and stress Equation (17) is 7.4590 MPa, with an error of about 1.47% compared with the simulation result. It can be seen from the mesh diagram that there is a neutral plane with a stress and strain state of 0 at the middle position of the prepreg tow subjected to traction rotation torque, and the tow on both sides of the neutral plane is in compression and tension states, respectively, and is symmetrical with respect to the neutral plane.

Secondly, the formation of wrinkles when the prepreg tow is laid at different angles is simulated in the post processor. The edge to be laid is set to rotate 10° around the fixed edge, and the length of the laid tow is 100 mm, and the calculated bending radius is 572.958 mm. It can be seen from Figure 10 that there are out of plane wrinkles with equal spacing distribution on the compressed side, and the buckling deflection is approximately sinusoidal, while there are no forming defects on the tensile side of the tow, which fits well with the mold. In conclusion, the distribution of defects is consistent with the theoretical model.

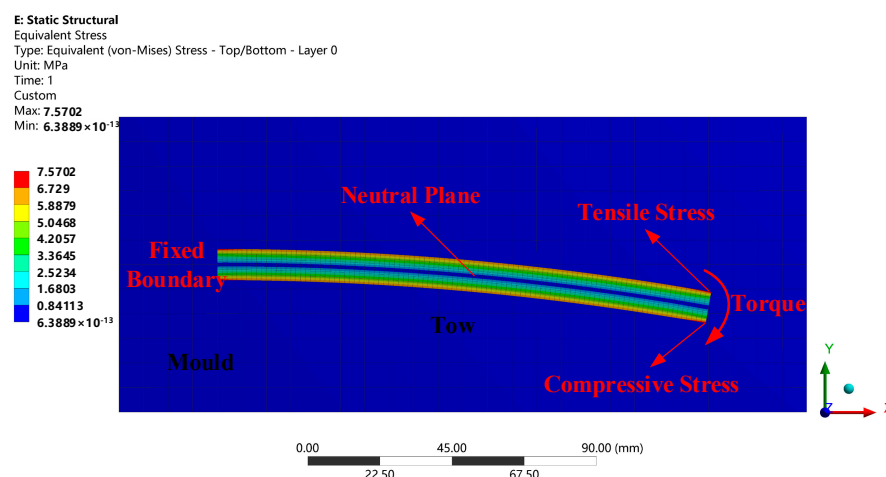


Figure 9. Simulation results of tangential stress.

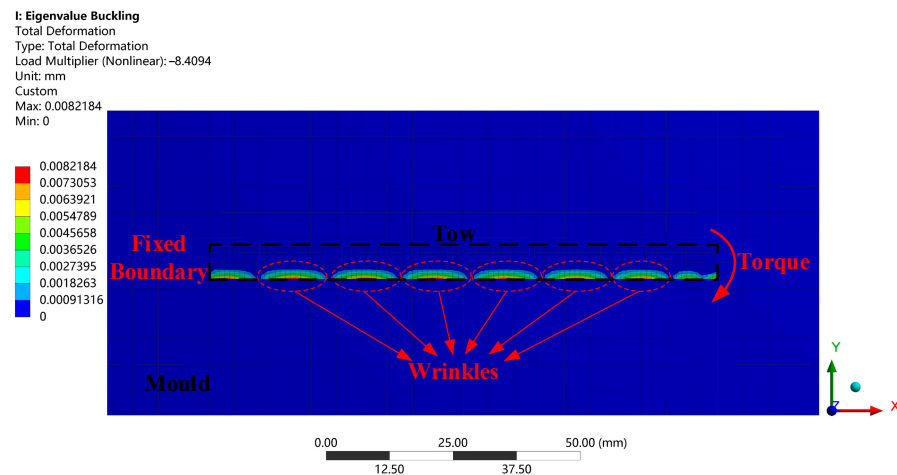


Figure 10. Simulation results of tow buckling.

4.3. Influence of Material Parameters

Since the main purpose of this section is to establish the corresponding relationship between the material parameters of the prepreg tow and the critical buckling radius, the influence of the laying process parameters, such as compaction force, can be excluded to simplify the model. The coefficient β can be set to 0, and the critical buckling radius Equation (18) can be simplified as:

$$r_{cr} = \frac{6L^2b^2}{\pi^5d_1^3h^2} \quad (19)$$

Figure 11 shows the relationship between the length of the tow with different widths and the critical buckling radius. The critical buckling radius increases with the length and is sensitive to the change in width. When the width of the tow is narrow, the change in the buckling radius with the length is small. When the width is increased to 1 inch, the increase in the laying length will easily lead to the formation of defects in the tow, such as wrinkles.

Figure 12 shows the relationship between the thickness of the tow with different widths and the critical buckling radius. With the increase of the thickness, the resistance of the prepreg tow to buckling is gradually enhanced, and the possibility of out of plane wrinkles is reduced. The thicker tow can realize large curvature bending without defects. In addition, the width of the tow still affects the sensitivity of the buckling radius to thickness.

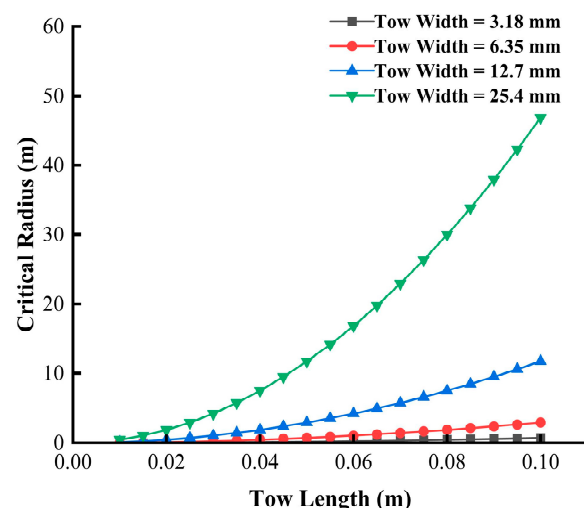


Figure 11. Critical steering radius of the tow plotted against length.

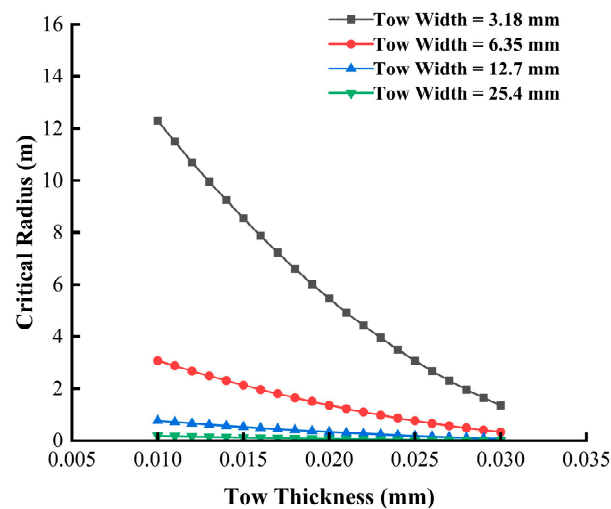


Figure 12. Critical steering radius of the tow plotted against thickness.

It can be seen from the above two line graphs that the width plays an important role in determining whether buckling occurs in VATS. The wider the width, the more likely the tow is to have wrinkles, warps and other defects during lateral bending, which is not conducive to the adaptation to complex curved surfaces. Therefore, when manufacturing complex structures such as aircraft engine blades and air inlets, it is preferred to use narrow prepreg tows for VATS.

5. Experimental Verification and Discussion

The robotic fiber placement shown in Figure 13 was used to perform the VATS experiments. The T700/epoxy resin prepreg tows produced by Guangwei Co., Ltd in Weihai, China are selected as the material, with a resin content of 33%, a tensile strength of 2300 MPa and a tensile modulus of 115 GPa. The ambient temperature of the test site is 26 °C. The area to be laid is heated to 35 °C by the infrared heating device integrated into the placement head, and the mold heating function is able to keep the temperature constant. After the laying of the first layer is completed, the quality of the layer should be observed immediately to eliminate the influence of multiple compaction after multi-layer laying on the wrinkles. Considering that it is difficult to detect the real-time adhesion coefficient between the tow and the mold, this paper mainly focuses on the qualitative verification of the buckling theoretical model.



Figure 13. Automated fiber placement experimental platform.

5.1. Influence of Steering Radii

Firstly, the influence of tow steering radius on the formation of defects such as wrinkles was explored through a group of experiments with different curvature radii. When the area to be laid is heated to 35 °C, the robotic placement will heat and lay the prepreg tow on the mold surface at a laying speed of 0.1 m/s and a compaction force of 50 N, and the laying length of the tow is set to 1 m. The 8 trajectories of this group of experiments are set as straight-line paths and curve paths with a steering radius of 20 m, 10 m, 5 m, 2.5 m, 1.5 m and 0.5 m (Figure 14).

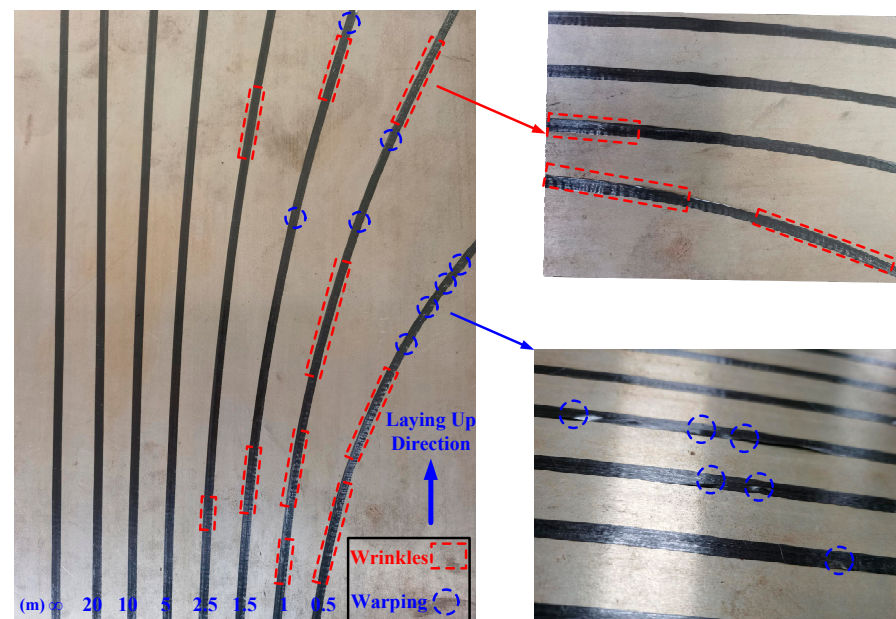


Figure 14. Results of experiment with different steering radii and close-up view of the defects.

The prepreg tow has obvious defects since the curvature radius of the trajectory is 2.5 m, and the specific form is the separation of the inner edge and the mold to varying degrees. When the radius of curvature is 2.5 m, a small range of wavy wrinkles appear on the inner side of the fiber tow. As the radius gradually decreases, the defects become more and more obvious, and the area where defects appear gradually increases. When the radius of curvature is 1.5 m, the wrinkles develop into warping, and there is a serious delamination between the tow and the mold. Until the radius reaches 0.5 m, the tow is in a buckling state, and continuous wrinkles are formed on the inner side with serious defects. Therefore, it can be proven that the corresponding relationship between the steering radius and the in-plane load (Equation (18)) is accurate; that is, as the radius decreases, the compression load on the inner side of the tow increases until it exceeds the critical buckling load, leading to defects, such as wrinkles, which are more likely to occur on the compressed side of the tow.

5.2. Influence of Compaction Force

According to the steering radius experiments, it can be concluded that the prepreg tow will produce wrinkles and other defects at a radius of 2.5 m under the force of 50 N. Therefore, the radius is set to 2.5 m and the temperature is kept at 35 °C in this group of experiments. The robotic placement applied different compaction forces and laid the tow at a speed of 0.1 m/s to verify the influence of compaction force on forming defects. The variation range of compaction force was set to be 20 N to 80 N, and the interval was 5 N. The results are shown in Figure 15.

With the increase of the compaction force, the obvious warpage phenomenon gradually disappears, and the range and frequency of wrinkles are also significantly reduced. This is because an appropriate pressure increase can make the resin flow better between the tow and the molding mold, inhibit the generation of bubbles, and make the prepreg fit

better. However, excessive pressure will cause low resin content between layers, affecting the bonding performance. It is proven that the adhesion performance between the tow and the mold can be increased by increasing the force, and the formation of buckling defects can be suppressed, which helps to reduce the in-plane load and decrease the critical buckling radius.

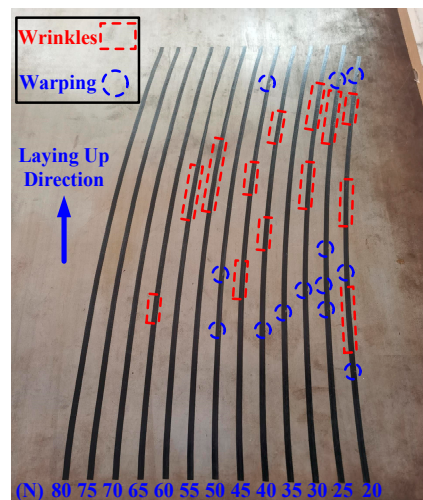


Figure 15. Results of experiment with different compaction forces.

5.3. Influence of Layup Rate

According to Equations (15) and (16), the laying rate also has an effect on the adhesion performance, in-plane load and critical buckling radius of the prepreg tow. The compaction force of the experiment was 50 N, the temperature was 35 °C, and the radius of curvature of the laying trajectory was 2.5 m. The laying speed ranged from 0.1 m/s to 0.5 m/s with an interval of 0.05 m/s.

In Figure 16, different laying speeds correspond to uneven forming quality. The faster the laying speed, the shorter the contact time between the compaction roller and the tow, which leads to a poor fit between the tow and the mold. In addition, the fast velocity leads to insufficient heating temperature in the placement area and poor fluidity and viscosity of the prepreg resin, which further reduces the bonding quality. In this case, the inhibition effect of tow adhesion on wrinkle formation is very poor. The actual results are consistent with the theoretical model; that is, excessive laying speed reduces the adhesion coefficient of the tow, so that a small in-plane compression load can cause buckling, wrinkles or even wavy warping.

Through the aforementioned laying experiments, the influence mechanism of forming process parameters on the formation of defects in VATS can be revealed, and the theoretical buckling model established above can be qualitatively verified. The theoretical calculation, simulation and experiment results are consistent, which proves the feasibility of applying Hertz's contact and tangential contact theories to optimize the variable angle tow buckling model based on Rayleigh–Ritz solution, minimum potential energy principle and viscoelastic foundation, and lays a theoretical foundation for the research of VATS technology and defect control method. However, due to the experimental conditions, there is no accurate measurement method for the viscosity of prepreg tow resin, so it is impossible to establish the quantitative relationship between the critical load and the process parameters. Future research can determine the resin viscosity of tow under specific temperature conditions through multiple groups of controlled variable experiments and then explore the characterization method of adhesion coefficient to realize the qualitative analysis and demonstration of the buckling model.

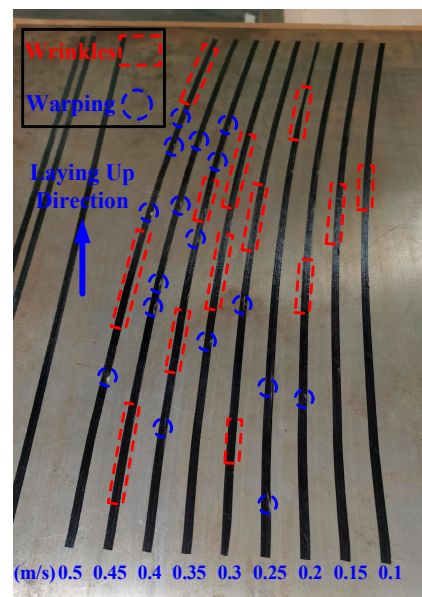


Figure 16. Results of experiment with different layup rates.

6. Conclusions

A buckling model including the width, thickness, adhesion coefficient and other material properties of the prepreg tow is proposed for the placement of complex composite structural parts in the aviation field. The critical in-plane load and buckling radius in VATS are solved by the Ritz method and the minimum potential energy principle based on more accurate boundary conditions and deflection functions. On this basis, the normal contact and tangential contact models of the compaction roller and the tow are innovatively established, so that the buckling model is improved by the theory of intimate contact and traction torsion without sliding, and factors such as the compaction force, laying speed and resin viscosity are introduced into the model, which is an important innovation point of this paper. In addition, a simulation model of VATS based on cohesion theory was established, and the distribution of compaction pressure as well as in-plane load was verified, which proved the feasibility of using viscoelastic foundation to characterize the adhesion of prepreg tow. Finally, the proposed theory and simulation models are verified by multiple groups of single factor laying experiments. It is proven that a proper increase in compaction force and a decrease in velocity can improve the adhesion performance of prepreg tow and reduce the critical radius in VATS.

Limited by the current experimental conditions and testing methods, this paper lacks research on the quantitative characterization methods and experimental verification of the adhesion coefficient. In addition, due to the temperature fluctuation, the corresponding relationship between process parameters and the critical buckling radius needs to be established. Future research will be devoted to exploring the relationship between the heating temperature and the formation of defects in VATS. In view that the resin viscosity of the prepreg tow is sensitive to temperature, and the heating process has a great influence on the adhesion coefficient of the tow, it is important to establish an accurate temperature field model to introduce the thermal effect into the buckling model to achieve high-quality placement. Furthermore, composite structures are composed of multiple layers, and each layer has undergone repeated compaction and heating processes. It is of great significance to study the effect of repeated placement on wrinkle formation in VATS for improving the manufacturing quality of aviation components and parts.

Author Contributions: Conceptualization, M.Y.; methodology, W.Z. and X.D.; validation, F.L. and M.Y.; writing—original draft preparation, M.Y. and F.L.; writing—review and editing, M.Y.; supervision, X.D. All authors have read and agreed to the published version of the manuscript.

Funding: This research was funded by Zhejiang Provincial Natural Science Foundation, grant number LD22E050011, Ningbo Key Projects of Science and Technology Innovation 2025 Plan, grant number 2022Z070, National Natural Science Foundation of China, grant No. 51575018 and National Natural Science Foundation of China, grant number 52205003.

Data Availability Statement: Not applicable.

Conflicts of Interest: The authors declare no conflict of interest.

References

- Gordon, T.; Xu, X.; Wisnom, M.R.; Kim, B.C. Novel tape termination method for automated fibre placement: Cutting characteristics and delamination suppression. *Compos. Part A Appl. Sci. Manuf.* **2020**, *137*, 106023. [\[CrossRef\]](#)
- Oromiehie, E.; Prusty, B.G.; Compston, P.; Rajan, G. Automated Fibre Placement based Composite Structures: Review on The Defects, Impacts and Inspections Techniques. *Compos. Struct.* **2019**, *224*, 110987. [\[CrossRef\]](#)
- Debout, P.; Chanal, H.; Duc, E. Tool path smoothing of a redundant machine: Application to Automated Fiber Placement. *Comput. Aided Des.* **2011**, *43*, 122–132. [\[CrossRef\]](#)
- Gurdal, Z.; Olmedo, R. In-plane response of laminates with spatially varying fiber orientations—Variable stiffness concept. *AIAA J.* **1993**, *31*, 751–758. [\[CrossRef\]](#)
- Lopes, C.S.; Gürdal, Z.; Camanho, P.P. Tailoring for strength of composite steered-fibre panels with cutouts. *Compos. Part A Appl. Sci. Manuf.* **2010**, *41*, 1760–1767. [\[CrossRef\]](#)
- Matsuzaki, R.; Mitsui, K.; Hirano, Y.; Todoroki, A.; Suzuki, Y. Optimization of curvilinear fiber orientation of composite plates and its experimental validation. *Compos. Struct.* **2020**, *255*, 112956. [\[CrossRef\]](#)
- Maung, P.T.; Prusty, G.B.; Phillips, A.; St John, N.A. Curved fibre path optimization for improved shape adaptive composite propeller blade design. *Compos. Struct.* **2021**, *255*, 112961. [\[CrossRef\]](#)
- Marques, F.D.; Natarajan, S.; Ferreira, A. Evolutionary-based aeroelastic tailoring of stiffened laminate composite panels in supersonic flow regime. *Compos. Struct.* **2017**, *167*, 30–37. [\[CrossRef\]](#)
- Bakhshi, N.; Hojjati, M. Time-dependent wrinkle formation during tow steering in automated fiber placement. *Compos. Part B Eng.* **2019**, *165*, 586–593. [\[CrossRef\]](#)
- Zhao, C.; Xiao, J.; Huang, W.; Huang, X.; Gu, S. Layup quality evaluation of fiber trajectory based on prepreg tow deformability for automated fiber placement. *J. Reinf. Plast. Compos.* **2016**, *35*, 1576–1585. [\[CrossRef\]](#)
- Wehbe, R.; Tatting, B.; Rajan, S.; Harik, R.; Sutton, M.; Gürdal, Z. Geometrical Modeling of Tow Wrinkles in Automated Fiber Placement. *Compos. Struct.* **2020**, *246*, 112394. [\[CrossRef\]](#)
- Punera, D.; Mukherjee, P. Recent developments in manufacturing, mechanics, and design optimization of variable stiffness composites. *J. Reinf. Plast. Compos.* **2022**. [\[CrossRef\]](#)
- Beakou, A.; Cano, M.; Cam, J.; Verney, V. Modelling slit tape buckling during automated prepreg manufacturing: A local approach. *Compos. Struct.* **2011**, *93*, 2628–2635. [\[CrossRef\]](#)
- Matveev, M.Y.; Schubel, P.J.; Long, A.C.; Jones, I.A. Understanding the buckling behaviour of steered tows in Automated Dry Fibre Placement (ADFP). *Compos. Part A Appl. Sci. Manuf.* **2016**, *90*, 451–456. [\[CrossRef\]](#)
- Belhaj, M.; Hojjati, M. Wrinkle formation during steering in automated fiber placement: Modeling and experimental verification. *J. Reinf. Plast. Compos.* **2018**, *37*, 396–409. [\[CrossRef\]](#)
- Bakhshi, N.; Hojjati, M. An experimental and simulative study on the defects appeared during tow steering in automated fiber placement. *Compos. Part A Appl. Sci. Manuf.* **2018**, *113*, 122–131. [\[CrossRef\]](#)
- Im, S.H.; Huang, R. Evolution of Wrinkles in Elastic-Viscoelastic Bilayer Thin Films. *ASME J. Appl. Mech.* **2005**, *72*, 955–961. [\[CrossRef\]](#)
- Wang, Q.; Zhao, X. A three-dimensional phase diagram of growth-induced surface instabilities. *Sci. Rep.* **2015**, *5*, 8887. [\[CrossRef\]](#)
- Shen, J.; Pirrera, A.; Groh, R.M. Building blocks that govern spontaneous and programmed pattern formation in pre-compressed bilayers. *Proc. R. Soc. A* **2022**, *478*, 20220173. [\[CrossRef\]](#)
- Mantell, S.C.; Springer, G.S. Manufacturing Process Models for Thermoplastic Composites. *J. Compos. Mater.* **1992**, *26*, 2348–2377. [\[CrossRef\]](#)
- Zhao, P.; Shirinzadeh, B.; Shi, Y.; Cheuk, S.; Leon, C. Multi-pass layup process for thermoplastic composites using robotic fiber placement. *Robot. Comput. Integr. Manuf.* **2018**, *49*, 277–284. [\[CrossRef\]](#)
- Çelik, O.; Peeters, D.; Dransfeld, C.; Teuwen, J. Intimate contact development during laser assisted fiber placement: Microstructure and effect of process parameters. *Compos. Part A Appl. Sci. Manuf.* **2020**, *134*, 105888. [\[CrossRef\]](#)
- Jiang, J.; He, Y.; Wang, H.; Ke, Y. Modeling and experimental validation of compaction pressure distribution for automated fiber placement. *Compos. Struct.* **2020**, *256*, 113101. [\[CrossRef\]](#)
- Li, J.F.; Song, C.; Wang, X.F.; Xiao, J. Study on pressure control of automated fiber placement process. In Proceedings of the 19th International Conference on Composite Materials, Montreal, QC, Canada, 28 July–2 August 2013.
- Sauer, R.A. A Survey of Computational Models for Adhesion. *J. Adhes.* **2016**, *92*, 81–120. [\[CrossRef\]](#)